

This article was downloaded by:

On: 14 January 2011

Access details: *Access Details: Free Access*

Publisher *Taylor & Francis*

Informa Ltd Registered in England and Wales Registered Number: 1072954 Registered office: Mortimer House, 37-41 Mortimer Street, London W1T 3JH, UK



## Molecular Simulation

Publication details, including instructions for authors and subscription information:

<http://www.informaworld.com/smpp/title~content=t713644482>

### Carbon nanotube assisted water self-diffusion across lipid membranes in the absence and presence of electric fields

J. -A. Garate<sup>a</sup>; N. J. English<sup>a</sup>; J. M. D. MacElroy<sup>a</sup>

<sup>a</sup> The SEC Strategic Research Cluster and the Centre for Synthesis and Chemical Biology, UCD School of Chemical and Bioprocess Engineering, University College Dublin, Dublin 4, Ireland

First published on: 21 September 2010

**To cite this Article** Garate, J. -A. , English, N. J. and MacElroy, J. M. D.(2009) 'Carbon nanotube assisted water self-diffusion across lipid membranes in the absence and presence of electric fields', *Molecular Simulation*, 35: 1, 3 – 12, First published on: 21 September 2010 (iFirst)

**To link to this Article:** DOI: 10.1080/08927020802353491

**URL:** <http://dx.doi.org/10.1080/08927020802353491>

PLEASE SCROLL DOWN FOR ARTICLE

Full terms and conditions of use: <http://www.informaworld.com/terms-and-conditions-of-access.pdf>

This article may be used for research, teaching and private study purposes. Any substantial or systematic reproduction, re-distribution, re-selling, loan or sub-licensing, systematic supply or distribution in any form to anyone is expressly forbidden.

The publisher does not give any warranty express or implied or make any representation that the contents will be complete or accurate or up to date. The accuracy of any instructions, formulae and drug doses should be independently verified with primary sources. The publisher shall not be liable for any loss, actions, claims, proceedings, demand or costs or damages whatsoever or howsoever caused arising directly or indirectly in connection with or arising out of the use of this material.

## Carbon nanotube assisted water self-diffusion across lipid membranes in the absence and presence of electric fields

J.-A. Garate, N.J. English and J.M.D. MacElroy\*

*The SEC Strategic Research Cluster and the Centre for Synthesis and Chemical Biology, UCD School of Chemical and Bioprocess Engineering, University College Dublin, Belfield, Dublin 4, Ireland*

*(Received 9 May 2008; final version received 17 July 2008)*

Water self-diffusion has been investigated by molecular dynamics (MD) simulation through armchair single-walled carbon nanotubes (SWCNTs) implanted in 1-palmitoyl-2-oleoyl-*sn*-glycero-3-phosphatidylcholine (POPC) membrane patches. Four systems were investigated, each containing one of (5,5), (6,6), (8,8) and (11,11) CNTs with diameters of 6.89, 8.20, 11.04 and 15.02 Å respectively and a length of 36.9 Å, oriented normal to the membrane. The CHARMM27 potential was used, in conjunction with TIP3P water, with particle-mesh Ewald electrostatics. Equilibrium and non-equilibrium MD simulations were performed in the respective absence and presence of a static electric field with an intensity of 0.0065 V/Å, applied along the axis normal to the membrane, i.e. approximately along the axis of the CNTs. It was found that the permeation rate of tracer water molecules was enhanced from 1.13 to 2.6 particles per nanosecond in the presence of the field in the case of (5,5) CNT, whilst the permeation rate per unit area declined in the larger nanotubes vis-à-vis equilibrium zero-field conditions. Single-file diffusion was observed in the (5,5) and (6,6) cases, compared with classical diffusion in the larger pores. From an analysis of the molecular dipole moment distributions, the number of water molecules present in the CNTs and the hydrogen-bonding characteristics of water inside the CNTs and at their mouth, these trends have been rationalised. A significant decrease in the fluctuations in the number of water molecules in the (5,5) CNT due to an enhanced dipole alignment in the electric field resulted in an increased rate of incorporation of the water molecules into this CNT, whereas a sharper alignment of the water dipoles with the field coupled with the greater rotational freedom of the water molecules in the (6,6) nanotube tended to reduced water self-diffusion.

**Keywords:** water self-diffusion; carbon nanotubes, lipid membranes

### 1. Introduction

In the last 25 years, the molecular simulation of transport process in inhomogeneous media and nanoporous structures, ubiquitous to many physical, chemical and biological systems, has grown rapidly. In particular, recent work has focussed on water transport within biological membranes (for example aquaporins [1,2], gramicidin-like channels [3]) and simplified models of these systems (single carbon nanotubes (CNTs) or arrays of CNTs [1,4–10]). The work on CNTs is of significant interest in that these materials display a simplicity of behaviour which permits a clearer understanding of the mechanics of the transport processes taking place in more complex biological media. For example, Zhu and Schulten [5] simulate a hexagonal array of (6,6) armchair CNTs with four basic charge conformations including two interesting bipolar charge configurations that are considered to be representatives of the electrostatic fields in biological channels (most notably as simple models of aquaporins). The authors observe that the charge electrostatic fields within the channels give rise to specific water dipole orientations that ultimately have a significant effect on the permeation rates. The observed rates are discussed in light

of the continuous-time random walk (CTRW) model of Berezhkovskii and Hummer [4] which predicts that the permeation rate,  $j$ , for water tracer molecules undergoing unidirectional single file diffusion is (see also [1])

$$j = \frac{pv_w}{2} \Delta c_{tr} = \frac{v_w k}{2(N+1)} \Delta c_{tr} = \frac{v_w k_0}{N+1} \Delta c_{tr}, \quad (1)$$

where  $v_w$  is the average volume of a single water molecule,  $p$  and  $k$  are the number of bi-directional permeation events per unit time and the bi-directional hopping rate, respectively,  $k_0$  is the unidirectional hopping rate and  $N$  is the number of water molecules in the channel. In [1,4,5] the average hopping rate is generally related to the intrapore self-diffusion coefficient,  $D_p$ , by

$$k = 2D_p/a^2, \quad (2)$$

where  $D_p$  is computed from the mean-square displacement of the water molecules inside the nanotubes and  $a$  is the average spacing between the water molecules. The results reported by Zhu and Schulten for the (6,6) channels 1.34 nm in length (with loadings corresponding to five water molecules) were in good agreement with the above expressions.

\*Corresponding author. Email: don.macelroy@ucd.ie

Additional studies [1,6,7] have examined pressure-driven water flows across membranes composed of arrays of (6,6) single file CNTs and larger CNTs (see [8] and others cited therein). The results in all the cases demonstrate that the convective flows are very high and that the transport process is close to being frictionless within the nanotubes in view of their relatively smooth walls at an atomic scale. While convective flow is not investigated in the work to be reported below the observation of the absence of any significant barriers to transport within the CNTs will be relevant to the discussion of the results to be presented later.

In this paper, we report further studies of unidirectional single file diffusion of water within (5,5) and (6,6) CNTs and classical diffusion of water in (8,8) and (11,11) CNTs. The latter provide insight into the transitional behaviour of the diffusional flux as the transport mechanism changes from single file to classical. On the other hand, the studies on (5,5) and (6,6) CNT will serve to assess the validity of Equation (1) in light of recent results reported by Li et al. [9]. Computations are also reported for diffusion in the presence of a static electric field highlighted the shortcomings in a simplified approach described by Equations (1) and (2). The CNTs were embedded in a bilayer membrane to imitate the influence of a relevant biological ‘background’ on the diffusional properties of water. Although the explicit influence of the head groups upon water diffusion is beyond the scope of this paper, we intend to examine this in some detail in future work.

## 2. Simulation methods and modelling

### 2.1 Simulation methods

All simulations were performed using the MD program NAMDv2.6b [11] and the CHARMM27 parameter set [12]. The rigid TIP3P water model [13] was used, since the CHARMM27 set was parameterised in conjunction with this potential. Four periodically replicated simulation cells were investigated, with each one consisting individually, respectively, of (5,5), (6,6), (8,8) and (11,11) armchair single-walled carbon nanotubes (SWCNT’s) with diameters of 6.89, 8.20, 11.04 and 15.02 Å and an approximate length of 36.9 Å; each was embedded in a 1-palmitoyl-2-oleoyl-*sn*-glycero-3-phosphatidylcholine (POPC) membrane patch, with layers of solvation water molecules of about 10 Å in length in the  $+z$  and  $-z$  directions (i.e. ‘above’ and ‘below’ the membrane patch, *cf.* Figure 1). The finite-size SWCNTs were constructed using the program CoNTubv1.0 [14], with each atom of the CNT modelled as a neutral  $sp^2$  aromatic carbon, with uncapped ends. For all of the systems, the POPC membrane plane was placed in the  $x-y$  plane and the axis normal to the membrane was along the  $z$ -direction with the CNT oriented along the normal to the membrane. The periodic cell size for the (5,5) and (6,6) CNT cases was  $35 \times 35 \times 70 \text{ Å}^3$  with total atom numbers of 8780 and

8415, respectively, whilst the (8,8) and (11,11) CNT systems consisted of a periodic cell of  $45 \times 45 \times 70 \text{ Å}^3$  with 13,882 and 13,659 atoms, respectively. Each of these systems was built using the program VMDv1.86 [15].

The particle mesh-Ewald method [16] was used to compute long-range electrostatics to within a relative tolerance of  $1 \times 10^{-6}$ ; it was found that a real-space screening coefficient of  $0.258 \text{ Å}^{-1}$  and grid spacings in the 0.9–1 Å range of in each Cartesian direction offered this desired level of accuracy together with close-to-optimal execution speed. A cut-off distance of 12 Å was applied to real-space Ewald interactions. The same value was used for van der Waals interactions, with a smooth switching function applied thereto between 10 and 12 Å. The SHAKE algorithm [17] was applied to constrain the bond lengths to the hydrogen atoms and to maintain the rigid TIP3P geometry. A time step of 1 fs was used with the velocity Verlet scheme [18]. For MD in the NVT ensemble, Langevin dynamics [19] was applied with a set point of 300 K and a damping coefficient of  $1 \text{ ps}^{-1}$ . For MD in the NPT ensemble, the Nose–Hoover method was applied [20] with an anisotropic cell variation, using Langevin dynamics for piston fluctuation control [21], with set points of 1 atm and 300 K. The hydrogen bonds were identified by geometric criteria: a water pair is considered to be hydrogen bonded if the oxygen–oxygen distance is less than 3.5 Å and the  $\text{O–H} \cdots \text{O}$  angle is greater than  $150^\circ$ , with all  $\text{O–H} \cdots \text{O}$  angles classified as being between  $0^\circ$  and  $180^\circ$  [22].

Prior to production simulations, a 1 ns NPT relaxation run was performed with CNT atoms fixed and the lipid bilayer and water molecules moving freely. Following this, the CNT atoms were released slowly, maintaining a harmonic constraint thereon with a coefficient of  $1 \text{ kcal/mol Å}^2$ . This coefficient was reduced every 100 ps for 0.4 ns down to 1.5, 1.0 and  $0.5 \text{ kcal/mol Å}^2$ . After initial relaxation, equilibrium MD simulations were performed in the NPT ensemble on the systems containing the (5,5) and (6,6) CNTs for 30 ns, and for 20 ns in the case of the (8,8) and (11,11) CNTs, whilst maintaining a light harmonic constraint on the CNT atoms (with a coefficient of  $0.5 \text{ kcal/mol Å}^2$ ). The first 5 ns were considered as further relaxation, keeping the rest of the simulation time as production run.

To investigate the influence of the external static electric fields on water self-diffusion, non-equilibrium MD simulations were carried out in an electrical field with an intensity of  $0.0065 \text{ V/Å}$  applied in the  $-z$ -direction. In this case, the force exerted by the field on partial atomic charges  $q_{ia}$  is given by

$$f_{ia} = q_{ia}E.$$

After observing an instability of the lipid bilayer at substantially larger field intensities (of the order of  $0.1 \text{ V/Å}$ ), the value of  $0.0065 \text{ V/Å}$  was selected. It was

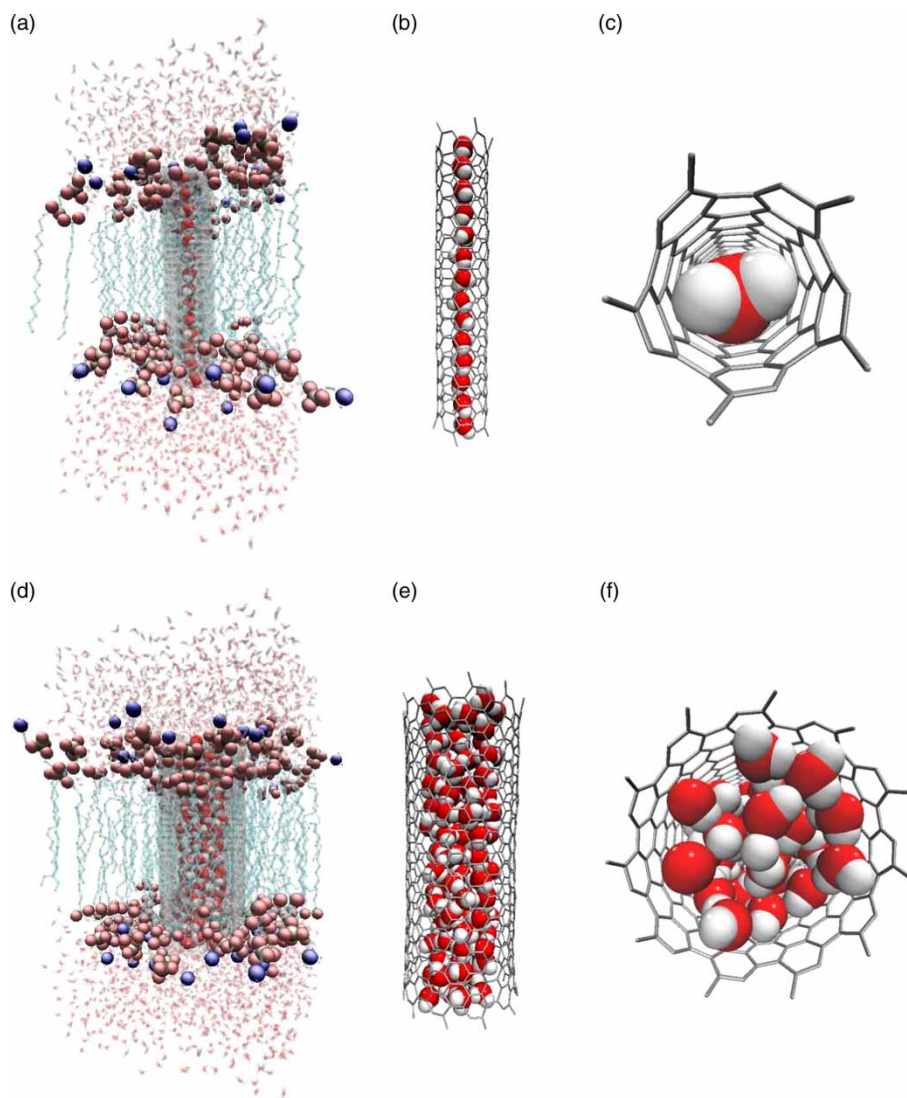


Figure 1. (a and d) Periodic cells simulated for the (5,5) CNT and (11,11) CNT systems respectively: in silver transparent rendering is the CNT with the waters inside represented as van der Waals oxygen and hydrogen spheres. The aliphatic chains of the membrane are shown to the left and right of the CNTs and the polar head groups are explicitly shown at the top and bottom of the aliphatic chains. Sticks at the top and bottom of the figures represent the bulk water. (b and e) Side view of the CNTs, (5,5) and (11,11) respectively with the water molecules rendered as van der Waals oxygen and hydrogen spheres inside the CNT. (c and f) Top view of the CNTs, (5,5) and (11,11) with the water molecules rendered as van der Waals oxygen and hydrogen spheres inside the CNT.

desired to assess a lower field intensity for longer periods of tens of nanoseconds, as this was in closer accord to experimental conditions, and the fully flexible bilayer was found to be stable under these field conditions. This field corresponds to a voltage difference of approximately 240 mV across the 3.7 nm membrane, which, although larger than typical membrane potentials of 60–100 mV, is still in the physiological range. The same configurations from the initial relaxation protocol were used as an input to the non-equilibrium simulations, except that they were carried out in the NVT ensemble to avoid any problems of too rapid dilation of the system volume in the relatively weak electric field.

No restraints were applied to the bilayer, while a light 0.5 kcal/mol  $\text{\AA}^2$  harmonic constraint was applied to the CNT atoms, in both the absence and the presence of the electric field. In particular, the neutral state of the CNT atoms led to no direct movement imparted thereon by the field (*cf.* equation above). Although Newsome and Sholl [23] have recommended with good justification the use of local thermostats to maintain appropriate isothermal conditions in the case of diffusion through fixed geometries, the mild harmonic restraints applied to the CNT in this study, coupled with the fully flexible bilayer, suggest that the thermostat used is reasonable. It is considered beyond the scope of this paper to conduct



a detailed study on the effects of thermostatting procedures on diffusion, but we intend to examine the influence of damping coefficients and the local and global application of thermostats on diffusion in future work.

Figure 2 illustrates the structure of the periodic cell for the analysis of the self-diffusion permeation rates for water within the CNTs described above. The periodic cell is imaged in all directions with a ‘black’ particle reservoir to the left and a ‘white’ particle reservoir to the right, both at a distance  $L$  from the respective CNT pore mouths. The steady-state counter-diffusion of both the species is monitored through the  $x - y$  plane located at  $z = 0$  within the CNT. ‘Black’ particles diffusing to the right are converted to ‘white’ once they enter the white reservoir and vice versa for the white particles. If a black particle diffuses from the left-hand reservoir across the periodic boundary at  $z = -L_c$  it enters as a white particle on the right-hand side. In all of the simulations conducted here  $L$  was taken as 0.6 nm.

## 2.2 Simplified diffusion/kinetic rate model

To model the diffusion process, consider the flux of the ‘black’ water molecules from left to right in Figure 2 (a similar analysis applies to ‘white’ diffusion). If the cross-sectional area in the bulk is  $A$  and the cross-section in the pore is  $A_p$  and  $L$  is the length of the mixing zone between the black reservoir and the pore mouth, then at steady state the net flow (particles per unit time) between the black reservoir and the outer perimeter of the CNT is simply

$$j_B = \frac{DA}{L}(c_1 - c_2), \quad (3)$$

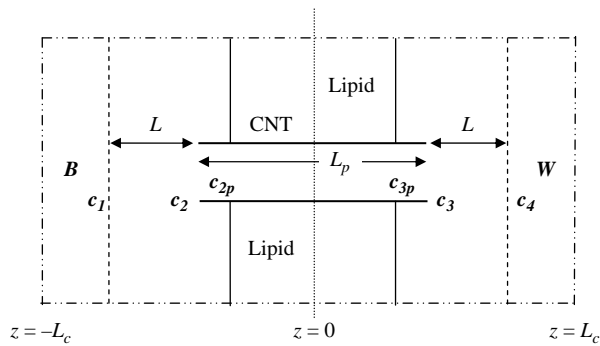


Figure 2. Schematic of the ‘black’ and ‘white’ water reservoirs on either side of the CNT, with the CNT oriented along the  $z$ -axis, normal to the membrane patch. The concentration of the black water molecules is specified at the edge of the black reservoir ( $c_1$ ), at the pore mouth ( $c_2$ ), just inside the pore ( $c_{2p}$ ), with analogous concentrations on the other side of the simulation cell (the positive  $z$ -coordinate half), i.e.  $c_{3p}$ ,  $c_3$  and  $c_4$ .  $L_c$  was 3.5 nm in all of the systems simulated.

where  $c_1$  is the concentration of black water molecules in the black reservoir and  $c_2$  is the concentration of black water molecules just outside the CNT pore mouth.

At the pore mouth, we consider a simple reversible rate process for the molecules to either enter the pore or return into the bath on the left, i.e. the net rate is

$$r_{2-2p} = k_f c_2 - k_r c_{2p}, \quad (4)$$

where  $k_i$  (forward and reverse hopping rates) is in units of  $s^{-1}$  and  $c_{2p}$  is the concentration of black water molecules just inside the CNT pore adjacent to the pore mouth. The above net rate is a volumetric measure (these rate constants will be determined to a great extent by the hydrogen bond structure and dynamics). Multiplying by a volume  $V_i$  (an interfacial volume corresponding to  $A_p \delta$  with  $\delta$  = length scale of the order of the molecular dimensions representing the scale of the concentration inhomogeneities), for steady-state conditions we have

$$\begin{aligned} V_i r_{2-2p} &= V_i (k_f c_2 - k_r c_{2p}) = V_i k_f (c_2 - \frac{1}{K_p} c_{2p}) = j_B \\ &= \frac{DA}{L} (c_1 - c_2). \end{aligned}$$

Eliminating  $c_2$  from this set of equations we have simply

$$j_B = \frac{p_1}{K_p} (K_p c_1 - c_{2p}), \quad (5)$$

where  $K_p$  is defined as  $k_f/k_r$  and  $p_1$  is the partial permeability for diffusive transport from the black reservoir to just inside the CNT:

$$\frac{1}{p_1} = \frac{L}{DA} + \frac{1}{k_f V_i}.$$

Defining a diffusion coefficient,  $D_p$ , within the pore (which is considered to exist in the same sense as proposed in [1,4,5] but which has a deeper meaning than indicated by the simple CTRW, as discussed towards the end of Section 3), we have

$$j_B = \frac{D_p A_p}{L_p} (c_{2p} - c_{3p}). \quad (6)$$

where  $L_p$  is the length of the pore and  $c_{3p}$  is the concentration of black water molecules just inside the CNT pore adjacent to the pore mouth near the white particle reservoir.

Also, for the right-hand side of the system it follows from Equation (5) that

$$j_B = \frac{p_1}{K_p} (c_{3p} - K_p c_4), \quad (7)$$

where  $c_4$  is the concentration of black water molecules in the white particle reservoir.

Now combining (5), (6) and (7) appropriately to eliminate the intermediate concentration terms between the reservoirs gives

$$j_B = p(c_1 - c_4),$$

where

$$\frac{1}{p} = \frac{2}{p_1} + \frac{L_p}{D_p K_p A_p} = \frac{2L}{DA} + \frac{2}{k_f V_i} + \frac{L_p}{D_p K_p A_p}. \quad (8)$$

A physical interpretation of Equation (8) is that the permeability is governed by a sum of mass transfer resistance terms due to bulk diffusion, incorporation into the pore mouth and intrapore diffusion. Normally one sets  $c_4 = 0$  and  $c_1 = c_{H_2O}$  = molar density of water in the bulk. The overall permeability can be simply determined from the MD simulations and one can eliminate the bulk diffusion ( $D/L$ ) terms by selecting different positions for the ‘black’ and ‘white’ reservoirs.

When compared with the simplified CTRW, it can be noted that implicit in the CTRW model is the assumption that  $L$  is sufficiently small to minimise the bulk-phase diffusional resistance while retaining a sub-nanometer range close to the pore mouth ( $\delta \sim a$ ) to ensure that entry/exit kinetics are fully taken into consideration. This condition with the additional assumption that the single file is considered to be densely packed leads to

$$L_p = Na; \quad \delta = a,$$

where  $a$  is a length scale characteristic of the size of the water molecules. Furthermore, the diffusion coefficient within the pore is also assumed in the CTRW model to be given by

$$D_p = \frac{a^2}{2\tau} = \frac{a^2}{2} k_r. \quad (9)$$

We further note here that we make the distinction that the intrapore hopping rate  $k$  is equal to  $k_r$ , i.e. the reverse rate constant in Equation (4). Within the pore, the forward and reverse hopping rate constants are equal; however, it is important to recognise that the forward rate constant

in Equation (4), which represents the rate at which water molecules enter the pore, is not equal to  $k_r$  and that for the CNTs under consideration here one may anticipate  $k_r > k_f$  or  $K_p < 1$ . Subject to these conditions and assuming the molecular volume  $v_w = aA_p$  we find

$$\begin{aligned} \text{Permeation rate} &= \frac{k_f a A_p}{2} \frac{1}{N+1} c_{H_2O} \\ &= \frac{v_w k_o}{N+1} \Delta c_{H_2O}, \end{aligned} \quad (10)$$

which is the simple CTRW result given in Equation (1). This analysis demonstrates the level of the assumptions involved in the CTRW approach. As noted above, in a more general setting, the in-pore forward hopping frequency is not the same as at the pore mouth. Furthermore, the more general model of Equation (8) applies to wide (i.e. multi-pass) pore conditions of arbitrary cross-sectional area and it is also simple to extend Equation (8) to include rate processes at other junctions (e.g. local charged sites) within the pore and to relate the rate constants to the energy barriers associated with the particle movement along the channel.

### 3. Results

The results for the steady-state unidirectional permeation rates (in number of water molecules per nanosecond) in both the absence and the presence of the static electric field are provided in Table 1 (note that the bulk resistance term  $2L/DA$  in Equation (8) is negligible in these studies amounting to approximately 1.3% of the overall resistance in the worst case for the largest pore). The zero-field results exhibit a monotonic increase with the pore radius as might be expected and the data have been scaled in the fourth column of the table to illustrate this. The influence of the electric field, however, is quite clearly evident in the third and last columns of this table. To gain insight into the phenomena that lead to these results let us first consider the zero-field data. In Table 2, we report the intrapore self-diffusion coefficients computed using

$$D_p = \lim_{t \rightarrow \infty} \frac{1}{2} \frac{d\langle(\Delta z)^2\rangle}{dt}$$

Table 1. Steady-state permeation rates.

Pore ( $d_p$ )	$j_0$ (ns <sup>-1</sup> )	$j_E$ (ns <sup>-1</sup> )	$p_0/A_p$ (nm ns <sup>-1</sup> ) <sup>a</sup>	$p_E/A_p$ (nm ns <sup>-1</sup> ) <sup>a</sup>
(5,5) (0.689 nm)	1.13 (0.19)	2.60 (0.87)	0.36	0.82
(6,6) (0.820 nm)	2.43 (0.91)	1.53 (0.57)	0.41	0.26
(8,8) (1.104 nm)	6.83 (1.4)	6.33 (0.43)	0.45	0.42
(11,11) (1.502 nm)	25.2 (1.8)	22.4 (1.7)	0.72	0.64

<sup>a</sup>The permeability  $p = j/c_w$  with  $c_w = 33.1 \text{ nm}^{-3}$ . The pore cross-sectional area employed here is  $(\pi/4)(d_p - 0.34)^2$  where  $d_p$  is the carbon centre–carbon centre diameter of the CNT given in the first column. 0.34 nm is the Lennard-Jones diameter of the carbon atoms.

Table 2. Intrapore diffusion and partitioning properties.

Pore	$D_{p0}$ (nm <sup>2</sup> ns <sup>-1</sup> )	$D_{pE}$ (nm <sup>2</sup> ns <sup>-1</sup> )	$p_0/D_{p0}A_p$ (nm <sup>-1</sup> )	$p_E/D_{pE}A_p$ (nm <sup>-1</sup> )	$K_{p0}^a$	$K_{pE}^a$
(5,5)	2.09 (0.31)	1.98 (0.12)	0.172	0.414	0.68	1.64
(6,6)	2.35 (0.23)	1.92 (0.17)	0.174	0.135	0.69	0.53
(8,8)	2.68 (0.19)	2.65 (0.48)	0.168	0.158	0.66	0.62
(11,11)	3.74 (0.24)	3.45 (0.54)	0.193	0.186	0.76	0.73

<sup>a</sup>The magnitude of  $a$  employed in Equation (11) to compute these values was 0.26 nm, the projected length for a given water molecule along the pore axis in the non-field single-file pores.

with the mean-square displacement (MSD) averaged over many time origins and determined from the particle trajectories for the period in which those particles originating at the centre of the pore remained within the pore (five sample bins were employed in computing the standard errors in each case reported in Table 2). In all cases, it was observed that after an initial sub-diffusion regime, the trajectories were linear (Fickian) for times  $t \geq 20$  ps (the MSDs for the two extreme cases of the (5,5) and (11,11) channels are provided in Figure 3 to illustrate the transition from sub-diffusion to the Fickian regime at approximately 20 ps). Rescaling the particle fluxes using the self-diffusion coefficients suggests that the intrapore diffusion or hopping rate,  $k_r$  [see Equation (9)] controls the magnitude of the diffusion flux for all pore sizes including the single file and classical diffusion conditions.

As an aside, we would like to note that for colour diffusion the distinction between transport diffusivity and self-diffusivity is not required since both are strictly equal under these special conditions. Only if a physical difference exists between the two counterdiffusing species (e.g. mass, particle diameter/shape or potential interaction) will this distinction arise. The colour particle diffusivity  $D_p$  in Equation (8) is precisely the same as the self-diffusivity computed from the derivative of the single-particle mean-square displacement and is independent of concentration. Also in view of the ideality of this special mixture the Darken factor is simply equal to 1.0.

Furthermore, if we assume, in keeping with the simplified lattice theory for diffusion in liquids, that generally  $V_i = aA_p$  then Equation (8) may be expressed as follows after neglecting the bulk diffusion term

$$p = D_p K_p \frac{A_p}{a + L_p}. \quad (11)$$

From the second last column of Table 2 it is clear that since the ratio of the rate constants  $K_{p0} = k_f/k_r$  is essentially independent of the pore size for the three smallest pores, the pore-entry hopping rate is strongly coupled with the internal hopping rate within the pore in agreement with the earlier work on water transport within single file (6,6) CNTs [1,4–7]. The larger value for the (11,11) CNT reflects an approach to the limiting condition

$K_p \rightarrow 1$  as the fluid within the pore and at the pore mouth assume properties characteristic of the bulk state.

In the presence of the electric field the results shown in Tables 1 and 2 demonstrate that the pore-entry and intrapore hopping rates are to some extent decoupled particularly for the two single file pores (5,5) and (6,6). The drop in the permeation rate for the (6,6) pore is consistent with observations similar to those by Zhu and Schulten [5] for a model (6,6) CNT with fixed charges of  $-0.5e$  and  $+0.5e$  at the respective ends of their 1.34 nm long nanotube. The influence of the electric field on the probability distribution of the angle of the water dipoles with respect to the (positive)  $z$ -axis,  $\theta$ , within our (5,5) and (6,6) pores is illustrated in Figure 4. In agreement with Zhu and Schulten, we find that the orientational distributions of the dipoles in the absence of the field are symmetric with peaks at  $\pm 1$  demonstrating that the dipoles of all the water molecules in the single file simultaneously point either in the  $-z$  or  $+z$  directions. In the presence of the static

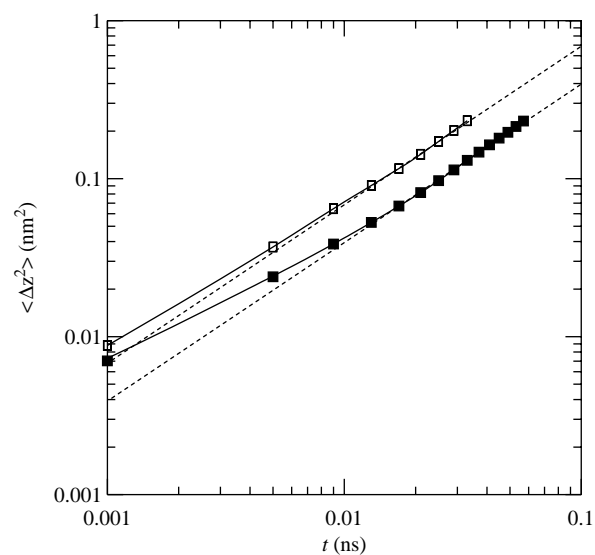


Figure 3. Axial mean square displacements as a function of time for individual water molecules confined within the pores. The filled squares are sample points for the (5,5) CNT and the open squares are for the (11,11) CNT. The dashed lines represent the linear (Fickian) limit. The results in both cases are for non-field conditions and the results in the presence of the e-field were found to be essentially the same.

e-field, the distribution is shifted almost entirely to the left of the diagrams. In the case of the (5,5) CNT there is a weak maximum in the region of  $\cos \theta = +1$ , while no such maximum exists for the (6,6) pore. The strongly

hindered rotational motion in the (5,5) pore is the reason for this since the water molecules fit very snugly within this CNT (the effective diameter of the (5,5) pore is  $(d_p - 0.34) = 0.349$  nm, which is nearly equal to the

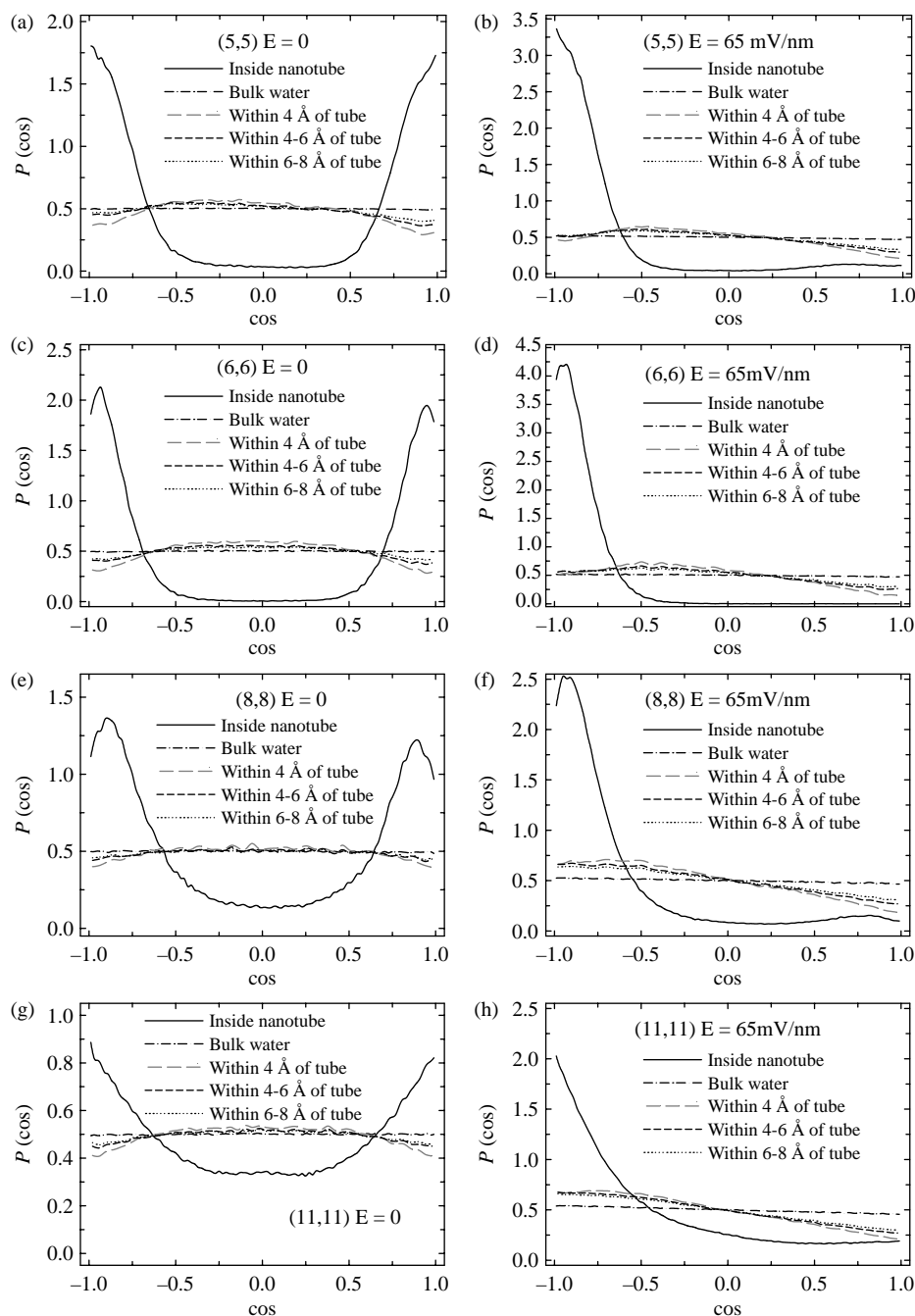


Figure 4. Normalised probability distributions of the cosine of the angle which the dipole moment vector of water molecules makes with the positive  $z$ -axis,  $\theta$ . The  $\cos \theta$  value is  $+1$  for a water dipole aligned along the  $+z$ -axis, and  $-1$  for a water molecule aligned along the  $-z$ -axis. The distributions are specified for the bulk water regions, i.e. those in the black and white reservoirs, inside the nanotube and within 4, 4–6 and 6–8 Å of the nanotube mouth. (a) (5,5) under zero-field conditions, (b) (5,5) in the field, (c) (6,6) under zero-field conditions, (d) (6,6) in the field, (e) (8,8) under zero-field conditions, (f) (8,8) in the field, (g) (11,11) under zero-field conditions and (h) (11,11) in the field.



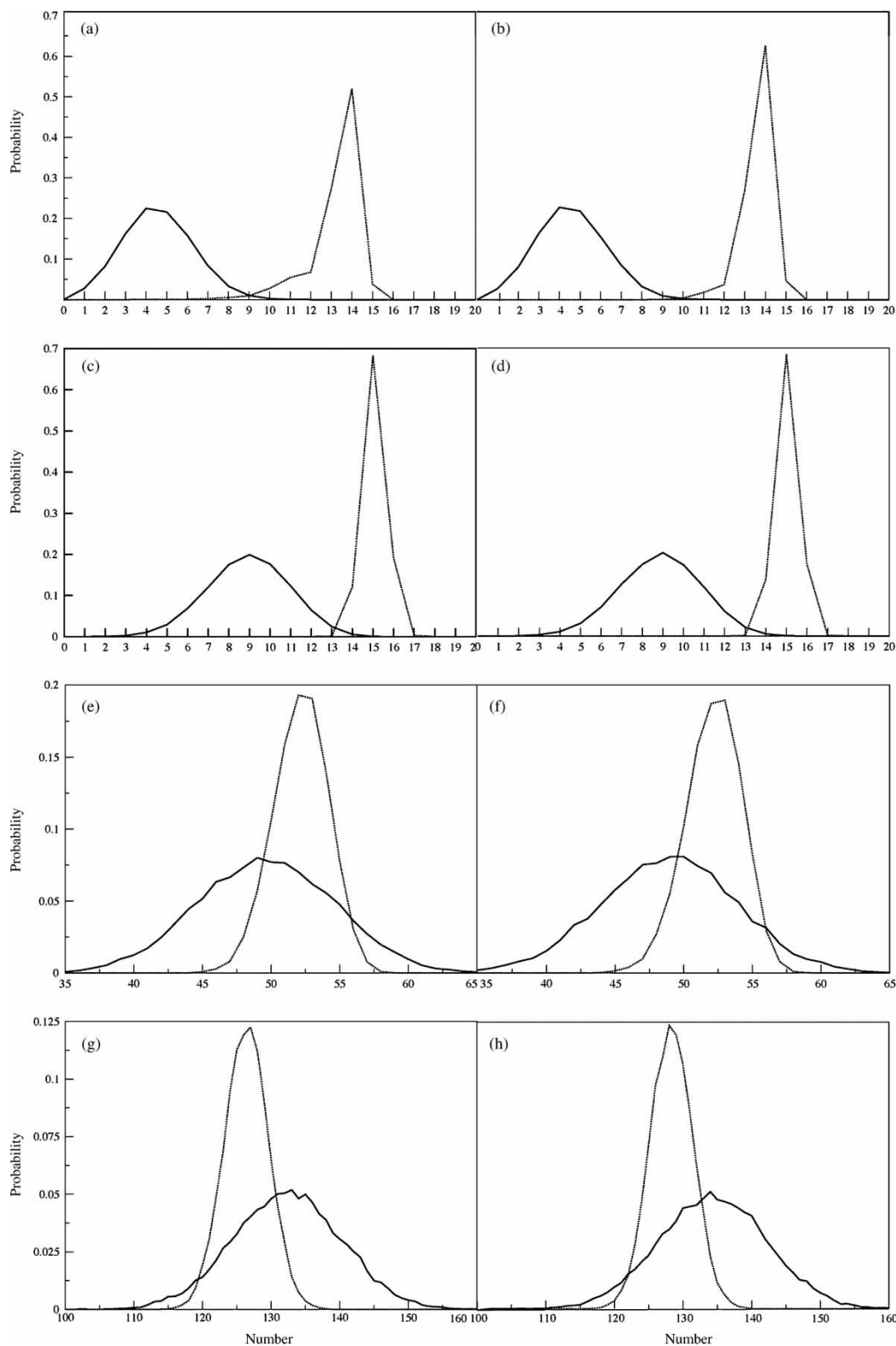


Figure 5. Normalised histograms of the number of hydrogen bonds (in black) and water molecules (in dotted grey) inside the CNTs during the MD simulations. (a) (5,5) under zero-field conditions, (b) (5,5) in the field, (c) (6,6) under zero-field conditions, (d) (6,6) in the field, (e) (8,8) under zero-field conditions, (f) (8,8) in the field, (g) (11,11) under zero-field conditions and (h) (11,11) in the field. The time series of these same values indicated a stationary situation without any appreciable drift.

oxygen Lennard-Jones diameter, 0.315 nm, for the TIP3P model – see, for example, Figure 1c). For the (6,6) pore the space is far less restricted with an effective pore diameter of 0.48 nm and the dipoles can readily align with the electric field.

The jump in the value for  $K_p$  shown for the (5,5) pore in the last column of Table 2 is closely related to the hindered rotational motion of the water molecules within this pore and to an additional feature of the water loading of the pore as shown in Figure 5. In this figure, we plot the distribution of the intrapore loadings and the number of hydrogen bonds for the entire MD simulations. With the exception of the (5,5) pore, the field has little effect on these properties. In the (5,5) pore, however, we note that the average number of water molecules within the pore in the absence of the field is generally lower than that when the field is turned on. In this pore, while H-bonding is the weakest, dipole alignment induced by the field results in a noticeable reduction in the fluctuations in particle numbers that are clearly observed in the absence of the field. A careful examination of a large number of snapshots of pore loadings in both the zero-field and the full-field simulations for this pore demonstrated that clusters of misaligned dipoles occurred with a high frequency in the zero-field case but were largely absent under the e-field conditions. This results in a greater frequency of jumps into the pore (high  $k_r$ ) with only a marginal, if any, effect on the reverse jump rate governed by  $k_r$  as implied by the diffusion coefficients  $D_{p0}$  and  $D_{pE}$ .

Before concluding, we consider a brief comparison of the non-field (6,6) results with those reported in Refs. [4,5,9]. The results we have obtained are qualitatively similar to those reported in [4,5]. Since the pore lengths differ by a factor of 3 we compare the hopping rates provided by  $D_p$ . In our case, we find  $k$  ( $= k_r$ ) = 69.5 ns<sup>-1</sup> while for similar thermodynamic conditions Berezhkovskii and Hummer [4] report a value of 76.9 ns<sup>-1</sup> and Zhu and Schulten [5] report 26.9 ns<sup>-1</sup>. It is of interest to note that our result is in very good agreement with that of Berezhkovskii and Hummer who employed the TIP3P model for water interactions and AMBER for the CNT, in contrast to the TIP3P/CHARMM potential modelling on which both our results and the results reported by Zhu and Schulten are based. We believe that the much lower hopping rates observed in [5] are due to the array of parallel nanotubes employed by the latter in their work. The single files of water within the 12 closely packed CNTs in [5] interact with one another via long-range electrostatic interactions causing friction that retards the rate of movement of the individual files (on an average half of the water files are moving counter to the remaining half).

A final point of interest is the qualitative verification of Equations (1) and (2) for our long pore results. Retaining the CTRW assumption that  $K_{p0} = 1$  and using only the results provided in Table 2 for  $D_p$  to estimate  $k$  with the hopping

length scale  $a = 0.26$  nm, we find for the (5,5) and (6,6) pores that Equation (1) predicts  $j = 1.59$  ns<sup>-1</sup> (5,5) and  $j = 3.39$  ns<sup>-1</sup> (6,6) in fair agreement with the full colour diffusion simulations (the primary reasons for the discrepancy rests with the assumption  $K_{p0} = 1$ ). This is in sharp contrast to the results reported by Li et al. [9], who suggest that the permeation rates are lower by a factor of 4 due to a pore-length dependence related to the decay in correlations associated with pore-entry and pore-exit hopping events. We observe no such dependence and also suggest that the lack of such a relationship (in contrast to the influence of pore-length suggested for stochastic diffusion processes in other sources [24–27]) does not exist due to the ‘frictionless’ nature of the water molecule interactions with the CNT pore walls. Our results do conform, however, to the ideal one-dimensional diffusion in a confined tubular space with specularly reflecting (axial momentum conserving) walls as suggested by the results of Lebowitz and Percus [28].

#### 4. Conclusions

The results reported in this work for single file pores in the absence of fields are in fair agreement with the CTRW of Berezhkovskii and Hummer [4] although discrepancies are observed particularly in the presence of electric fields. In this regard, it has been shown that the self-diffusion of water molecules through a (5,5) CNT embedded in a lipid bilayer is significantly enhanced by static electric fields, in contrast to that through CNTs of larger diameters. The electric field intensity of 0.0065 V/Å is weak in comparison with the previous molecular simulation studies employing static and time-varying fields [29,30] and is also weak relative to fields generated by charge distributions [5]. A significant decrease in the fluctuations in the number of water molecules in the (5,5) CNT upon application of the field facilitates the incorporation of a larger number of water molecules in the CNT, whereas the greater rotational freedom of water molecules in the (6,6) tube, and in larger CNTs, permits an enhanced alignment of their dipoles with the field resulting in a reduced water self-diffusion flux. In future work, we will examine this in greater detail and extend this work to investigate the influence of time-varying far infrared and microwave fields on the properties of water confined within model CNTs of various sizes in addition to the influence of head groups on water diffusion.

#### References

- [1] E. Tajkhorshid, F. Zhu, and K. Schulten, *Kinetic theory and simulation of single-channel water transport*, in *Handbook of Materials Modeling*, S. Yip ed., Springer, Netherlands, 2005, pp. 1797–1822.
- [2] M. Hashido, A. Kidera, and M. Ikeguchi, *Water transport in aquaporins: Osmotic permeability matrix analysis of molecular dynamics simulations*, Biophys. J. 93 (2007), pp. 373–385.

- [3] G. Portella, P. Pohl, and B.L. de Groot, *Invariance of single file water mobility in gramicidin-like peptidic pores as function of pore length*, Biophys. J. 92 (2007), pp. 3930–3937.
- [4] A. Berezhkovskii and G. Hummer, *Single-file transport of water through a carbon nanotube*, Phys. Rev. Lett. 064503 (2002), pp. 1–4.
- [5] F. Zhu and K. Schulten, *Water and proton conduction through carbon nanotubes as models of biological membranes*, Biophys. J. 85 (2003), pp. 236–244.
- [6] F. Zhu, E. Tajkhorshid, and K. Schulten, *Collective diffusion model for water permeation through microscopic channels*, Phys. Rev. Lett. 224501 (2004), pp. 1–4.
- [7] A. Kalra, S. Garde, and G. Hummer, *Osmotic water transport through carbon nanotube membranes*, Proc. Natl. Acad. Sci. USA 100 (2004), pp. 10175–10180.
- [8] S. Joseph and N.R. Aluru, *Why are carbon nanotubes fast transporters of water?* Nano Lett. 8 (2008), pp. 452–458.
- [9] J.-Y. Li, Z.-X. Yang, H.-P. Fang, R.-H. Zhou, and X.-W. Tang, *Effect of the carbon nanotube length on water permeability*, Chin. Phys. Lett. 24 (2007), pp. 2710–2713.
- [10] B. Mukherjee, P.K. Maiti, C. Dasgupta, and A.K. Sood, *Structure and dynamics of confined water inside narrow carbon nanotubes*, J. Nanosci. Nanotechnol. 7 (2007), pp. 1796–1799.
- [11] J.C. Phillips, R. Braun, W. Wang, J. Gumbart, E. Tajkhorshid, E. Villa, C. Chipot, R.D. Skeel, L. Kale, and K. Schulten, *Scalable molecular dynamics with NAMD*, J. Comp. Chem. 26 (2005), pp. 1781–1802.
- [12] A.D. MacKerell, Jr., D. Bashford, M. Bellott, R.L. Dunbrack, Jr., J.D. Evanseck, M.J. Field, S. Fischer, J. Gao, H. Guo, S. Ha et al., *All-hydrogen empirical potential for molecular modeling and dynamics studies of proteins using the CHARMM22 force field*, J. Phys. Chem. B 102 (1998), pp. 3586–3616.
- [13] W.L. Jorgensen, J. Chandrasekhar, J.D. Madura, R.W. Impey, and M.L. Klein, *Comparison of simple potential functions for simulating liquid water*, J. Chem. Phys. 79 (1983), pp. 926–935.
- [14] S. Melchor and J.A. Dobado, *CoNTub: An algorithm for connecting two arbitrary carbon nanotubes*, J. Chem. Inf. Comput. Sci. 44 (2004), pp. 1639–1646.
- [15] W. Humphrey, A. Dalke, and K. Schulten, *VMD – visual molecular dynamics*, J. Mol. Graph. Model. 14 (1996), pp. 33–38.
- [16] T. Darden, D. York, and L. Pedersen, *Particle mesh-Ewald: An Nlog(N) method for Ewald sums in large systems*, J. Chem. Phys. 98 (1993), pp. 10089–10092.
- [17] J.P. Ryckaert, G. Cicciotti, and H.J.C. Berendsen, *Numerical integration of the Cartesian equations of motion of a system with constraints: Molecular dynamics of n-alkanes*, J. Comp. Phys. 23 (1977), pp. 327–341.
- [18] M.P. Allen and D.J. Tildesley, *Computer Simulation of Liquids*, Clarendon Press, Oxford, 1987.
- [19] G.S. Grest and K. Kremer, *Molecular-dynamics simulation for polymers in the presence of a heat bath*, Phys. Rev. A 33 (1986), pp. 3628–3631.
- [20] G.J. Martyna, D.J. Tobias, and M.L. Klein, *Constant pressure molecular dynamics algorithms*, J. Chem. Phys. 101 (1994), pp. 4177–4189.
- [21] S.E. Feller, Y. Zhang, R.W. Pastor, and B.R. Brooks, *Constant pressure molecular dynamics simulation: The Langevin piston method*, J. Chem. Phys. 103 (1995), pp. 4613–4621.
- [22] A. Luzar and D. Chandler, *Effect of environment on hydrogen bond dynamics in liquid water*, Phys. Rev. Lett. 76 (1996), pp. 928–931.
- [23] D.A. Newsome and D.S. Sholl, *Predictive assessment of surface resistances in zeolite membranes using atomically detailed models*, J. Phys. Chem. B 109 (2005), pp. 7237–7244.
- [24] J.M.D. MacElroy and S.-H. Suh, *Self-diffusion in single file pores of finite length*, J. Chem. Phys. 106 (1997), pp. 8595–8597.
- [25] J.M.D. MacElroy and S.-H. Suh, *Equilibrium and nonequilibrium molecular dynamics studies of diffusion in model one-dimensional micropores*, Microporous Mesoporous Mat. 48 (2001), pp. 195–202.
- [26] K. Hahn and J. Karger, *Deviations from the normal time regime of single file diffusion*, J. Phys. Chem. B 102 (1998), pp. 5766–5771.
- [27] P.H. Nelson and S.M. Auerbach, *Self-diffusion in single file membranes is Fickian at long times*, J. Chem. Phys. 110 (1999), pp. 9235–9243.
- [28] J.L. Lebowitz and J.K. Percus, *Kinetic equations and density expansions: Exactly solvable one-dimensional system*, Phys. Rev. 155 (1967), pp. 122–138.
- [29] I.M. Svishchev and P.G. Kusalik, *Electrofreezing of liquid water: Microscopic insights*, J. Am. Chem. Soc. 118 (1996), pp. 649–654.
- [30] N.J. English and J.M.D. MacElroy, *Hydrogen bonding and molecular mobility in liquid water in external electromagnetic fields*, J. Chem. Phys. 119 (2003), pp. 11806–11813.